

# The Effect of Silicon Carbide Particulates on Tensile, Fatigue, Impact and Final Fracture Behaviour of 2618 Aluminium Alloy Matrix Composites

A.Sakthivel<sup>a</sup>, R. Palaninathan<sup>a</sup>,  
R. Velmurugan<sup>b,\*</sup> and Dr. P. Raghothama Rao<sup>c</sup>

<sup>a</sup>Department of Applied Mechanics, Indian Institute of Technology, Madras, Chennai-600036, Tamilnadu, India

<sup>b</sup>Composite Technology Centre, Indian Institute of Technology, Madras, Chennai -600036, Tamilnadu, India

<sup>c</sup>Scientist, CEMILAC, DRDO, Bangalore - 560 037

Received on 7/03/2010; Accepted on 2/06/2010

## Abstract

In this paper, the tensile, high cycle fatigue (HCF), Impact and fracture behaviour of Aluminium alloy 2618(AA 2618) reinforced with particulates of Silicon Carbide ( $\text{SiC}_p$ ) is discussed. AA 2618/ $\text{SiC}_p$  metal matrix composites (MMCs) were fabricated by two-step mixing of stir casting method followed by forging operation. A significant increase of the elastic modulus and tensile strength in the MMCs respect to the unreinforced alloys were evidenced by the tensile tests, while the elongation at fracture decreased. Temperature effects on the tensile properties at 120°C and 200°C were studied. The high cycle fatigue tests showed a marginal increase in fatigue life over the unreinforced alloys. A SEM analysis of the fracture surfaces showed that tensile failure was controlled by micro-void coalescence, interfacial decohesion and fracture of reinforcing particles, whereas fatigue was controlled by interfacial decohesion at the matrix-particle interface. The impact behaviour of the composites was affected by clustering of particles, particle cracking and weak matrix-reinforcement bonding. Agglomeration of the particles reduced the impact strength. The effect of particle size is invariant to the impact strength.

**Keywords:** Metal matrix composites, tensile tests, high-cycle fatigue, AA 2618,  $\text{SiC}_p$ .

## 1. INTRODUCTION

The strong demand for weight reduction in automobile and aircraft fabrication to employ low density materials requires the optimization of the design of products. Aluminium alloys are not sufficiently stiff or strong for many purposes and their reinforcement is often necessary. Aluminium metal matrix composites (Al MMCs) are outstanding candidates for these applications, owing to the high ductility of the matrix and the high strength of the hard reinforcing phase. Unfortunately, such materials are difficult to form, due to their intrinsic low ductility caused by the presence of the rigid reinforcing phase, usually  $\text{SiC}_p$  or  $\text{Al}_2\text{O}_3$  particles [1]. Aluminium alloys with a Copper: Magnesium weight ratio of 2:1 and higher are used for manufacturing a variety of age-hardenable structural alloys. The structural changes that occur during aging of these alloys have been extensively studied [2–5].

Aluminium metal matrix composites are being considered as a group of new advanced materials for their light weight, high strength, high specific modulus, low coefficient of thermal expansion and superior wear resistance properties. Combinations of these properties are not available in conventional materials [6–8]. Among the variety of manufacturing processes available for discontinuous metal matrix composites, stir casting is generally accepted as one of the promising routes. Its advantage lies

\*Corresponding Author. E-mail: ramanv@iitm.ac.in.

in its simplicity, flexibility and applicability to large quantity production. It is the most economical of all of the available routes for metal matrix composite production [6]. When the SiC<sub>p</sub> particles are added into the molten alloys, they are floating on the surface even though high specific density is due to high surface tension and poor wetting between the particles and melt. Gas layers over the surface of the melt are the main factor for the poor wettability. In a semisolid state, gas layer may disappear during manual stirring due to the collision between primary  $\alpha$  Al nuclei and particles. In the second mixing, uniform particle distribution was achieved above the liquidus temperature [9]. Hence, AA 2618/SiC<sub>p</sub> composites were fabricated by two-step mixing of stir casting method (First step: Particle addition in semi-solid state and Second step: Mechanical stirring at liquid state for uniform distribution). The two-step mixing has been applied successfully to improve the wettability and distribution of the particles.

With the development of metal matrix composites and their engineering applications in aerospace and automotive industries, their mechanical properties, mainly the tensile and fatigue behaviours are becoming very essential. The improvements in properties of tensile and fatigue with respect to unreinforced alloys strongly depend on the intrinsic properties of both the matrix and reinforcement (size, volume fraction and distribution) as well as on the mutual interaction between both the matrix and alloy. A major potential problem for particle reinforced composites is a non-uniform microstructure, often resulting from the manufacturing process, which can lead to the presence of clusters of particles, or regions without any reinforcement [10, 11]. The intrinsic material inhomogeneity can result in a wide scatter in both strength and ductility [12]. Complex relationships can exist between the fatigue properties and fracture characteristics of a discontinuous particulate – reinforced aluminium alloy MMC. These are dependent on the influences of: a) properties of the matrix (composition, ageing microstructure), b) properties of the particulate reinforcement phase (composition, morphology, size and volume fraction), c) influence of secondary processing on microstructure d) influence of test parameters such as nature, type and magnitude of loading and extent of cyclic plasticity [13, 14].

The literature survey indicates that although mechanical properties of particle reinforced aluminium matrix composites have been widely examined and little information is available on toughness and impact behaviour of these materials. The toughness and impact strength at room temperature of these composites have been investigated in several works using different materials and processing variables [15–18]. Work on the high and low temperature behaviour of Al<sub>2</sub>O<sub>3</sub> and SiC particles are limited [19–21]. The presence of hard SiC particles as a reinforcement in a ductile matrix of aluminium alloys (grades of 2123, 5083, 6063) decreased the impact toughness of the metal matrix composites [19]. Defects in the composite microstructure, such as clustering or particle agglomeration can act as a preferential site for crack nucleation and propagation. These nucleations coupled with particle failure by cracking and debonding at the particle interfaces allowing the microscopic cracks to grow rapidly and reduce the impact strength [19].

The objective of this paper is to understand the influence of the particulate reinforcement on the tensile, high cycle fatigue, impact and fracture behaviour of a 2618 aluminium alloy reinforced with particles of two sizes. The tensile deformation, high cycle fatigue response, impact resistance and final fracture behaviour of the composites are discussed in light of the influences of composite microstructural effects, matrix deformation characteristics, test temperature and nature of loading.

## 2. EXPERIMENTAL TECHNIQUE

### 2.1. Material system

In this study, aluminium alloy 2618 with a density of 2760 kg/m<sup>3</sup> was used as the matrix material and SiC<sub>p</sub> (silicon carbide) particles of two sizes 5–10  $\mu$ m (Average 7  $\mu$ m size) and 20–40  $\mu$ m (average 33  $\mu$ m size) with density of 3200 kg/m<sup>3</sup> were used as the reinforcement. The SiC particles were supplied by Carborundum Universal Ltd. The sizes of the SiC particles were determined using a Scanning Electron Microscope (SEM). The chemical composition of 2618 aluminium alloy is given in Table:1. Test specimens were made with 5 % and 10 % weight percentages (5P, 10P) of each type of particle. The particle sizes 5–10  $\mu$ m and 20–40  $\mu$ m are represented by the abbreviations ‘F’ and ‘C’ respectively.

**Table 1. Chemical composition (in %) of 2618 Al. alloy matrix**

Si	Mn	Cu	Fe	Mg	Ni	Ti	Ti-Zr	Zn	Al
0.2	0.2	2.3	1.1	1.5	1.1	0.2	0.25	0.15	Balance

## 2.2. Processing of MMC

Initially 2618 Al alloy was loaded into the crucible and heated to approximately 750°C till the entire alloy was melted. The SiC particles were preheated to 900°C for 1 hour before incorporation into the melt. The steel mould of size 150 × 120 × 30 mm<sup>3</sup> was used for the preparation of the cast blanks. The mould was also preheated to 200°C for 10 min. to obtain a uniform solidification. After the molten metal was fully melted, a degassing tablet was added to reduce the porosity. The melt was transferred into another crucible, which was separately heated to maintain 750°C temperature. The temperature of the melt was reduced to be in the range 610–650°C (Solidus - liquidus state) to incorporate the reinforcement. The preheated SiC particles were added at the rate of 20 gm/min with manual stirring. Magnesium (Max. 1% wt) was added to improve the wettability of the particles. The incorporation of the reinforcement particles within a semi-solid alloy is claimed to be advantageous because, the reinforcement entraps the semi-solid alloy, thereby avoiding particle agglomeration and settling. After the mixing of particle in the semisolid state, the temperature was increased to 720°C. The stirrer was lowered into the melt slowly to stir the molten metal at the speed of 500 rpm. The temperature was also monitored simultaneously during stirring. The mixture was poured into the mould. The maximum duration of mixing was 10 mins. The clearance of the stirrer from the bottom of the crucible was approximately 10 mm with the melt depth of 100 mm. The cast MMC billets were forged to break the cast structure to get equiaxed grains for the improvement of properties. The forging operation was carried out with 1000 tonne pneumatic hammer. For each operation, a temperature of 450°C was maintained for the duration of 2 hrs. The forged MMCs were then subjected to a heat treatment cycle (maintained 525°C for 2 hrs followed by water quenching and precipitate hardening at 175°C for 10 hrs). Specimens were prepared from the forged billet after heat treatment for testing.

## 2.3. Specimen preparation

The specimens were cut from the forged billets to the specification outlined in ASTM E8, ASTM E21, ASTM E23 and BS 3512 to carry out tensile, hot tensile, Izod impact and high cycle fatigue (HCF) tests respectively. The samples in an optical microscope (Nikon EPIPHOT-TME inverted Microscope) with metal power image analyzer were examined for reinforcement morphology and its distribution in the MMC along with other intrinsic microstructural features.

## 2.4. Mechanical testing and failure analysis

Tensile and hot tensile tests were carried out on a TIRA 2820S universal material testing machine with a modular test system. High cycle fatigue tests were conducted at 50 Hz and at a stress ratio ( $R = \sigma_{\text{minimum}}/\sigma_{\text{maximum}}$ ) of -1.0. The number of cycles to cause complete failure or separation was taken as fatigue life.

Fracture surfaces of the tensile, cyclically deformed and impact samples were examined in a Scanning Electron Microscope (SEM). Fractographic examinations were carried out by means of the SEM.

# 3. RESULTS AND DISCUSSION

## 3.1. Microstructure

Fig. 1 presents an optical micrograph showing the microstructure of the AA 2618/SiC<sub>p</sub>/10P/C composites. The silicon carbide particles in the 2618 aluminium alloy matrix were distributed uniformly (Fig.1a). The particle alignment is in the forging direction. Fig. 1(b) indicates the etched microstructure, which revealed that the matrix consists of fine grains with high fraction of second phase precipitates (Al<sub>2</sub>CuMg and FeNiAl<sub>2</sub>). Also the SiC particles are located both at the grain boundaries and inside the grains.

## 3.2. Tensile properties and fracture

The results of the tensile tests at room temperature and hot tensile test (at 120°C) for particle size 'F' and effect of weight percentage of particles relative to the unreinforced alloy are shown in Figs. 2 and 3. Fig. 2(a) indicates the variation of Young's modulus with the temperature for two weight percentages. From the figure, the Young's modulus of the MMC increases (8–19%) compared to the unreinforced alloy for both weight percentages of particles. The Young's modulus increases with weight percentage of particles. The increases in Young's modulus ranges are 8–15% and 12–19% for 5% and 10% weight of particles at room temperature, respectively. The same trend is observed even at 120°C temperature. Fig. 2(b) shows the variation of 0.2% proof strength (PS) with

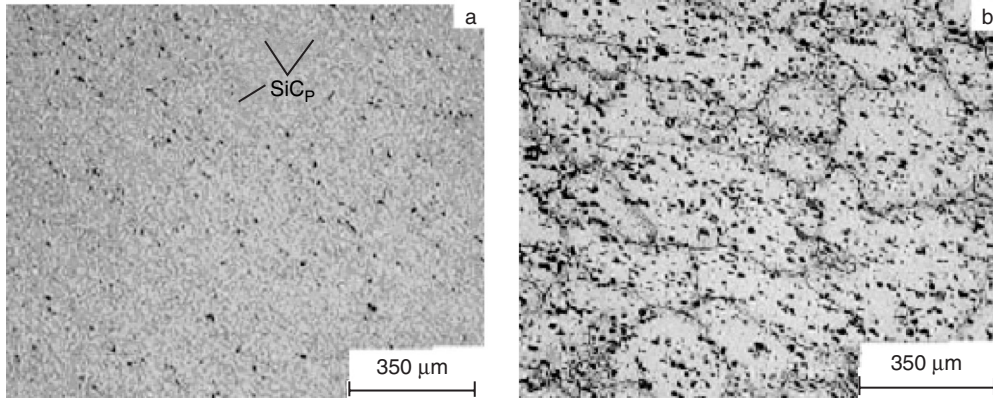


Figure 1. Optical micrographs illustrating the a) non-etched and b) etched microstructures of AA 2618/SiC<sub>p</sub>/10P/C composites.

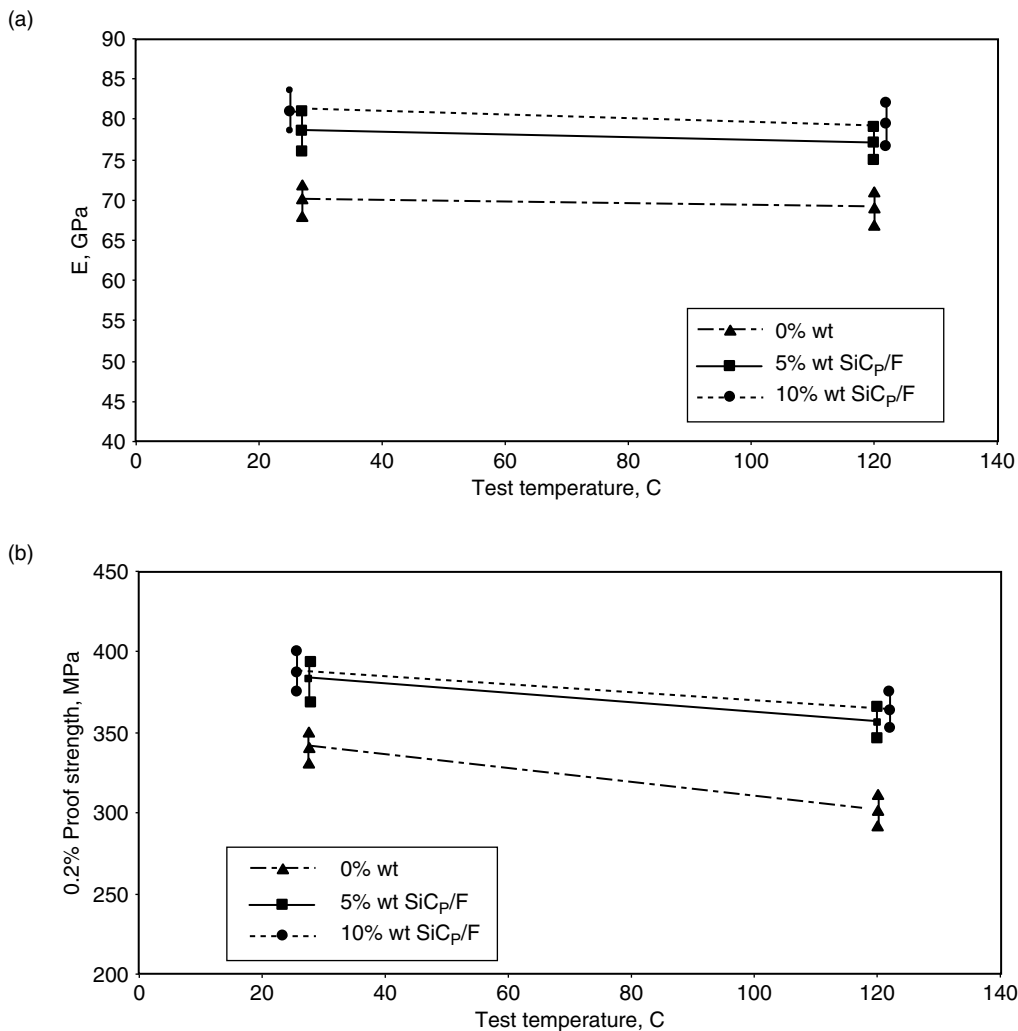


Figure 2. (a). Variation of Young's modulus with the temperature and % weight of particles. (b) Variation of 0.2% PS with the temperature and % weight of particles.

the temperature for two weight percentages of particles. From the figure, 0.2% proof strength of the MMC increases (8–18%) compared to the unreinforced alloy for both weight percentages of particles at room temperature. But, the increase is significant (15–25%) at 120°C condition. At the same time,

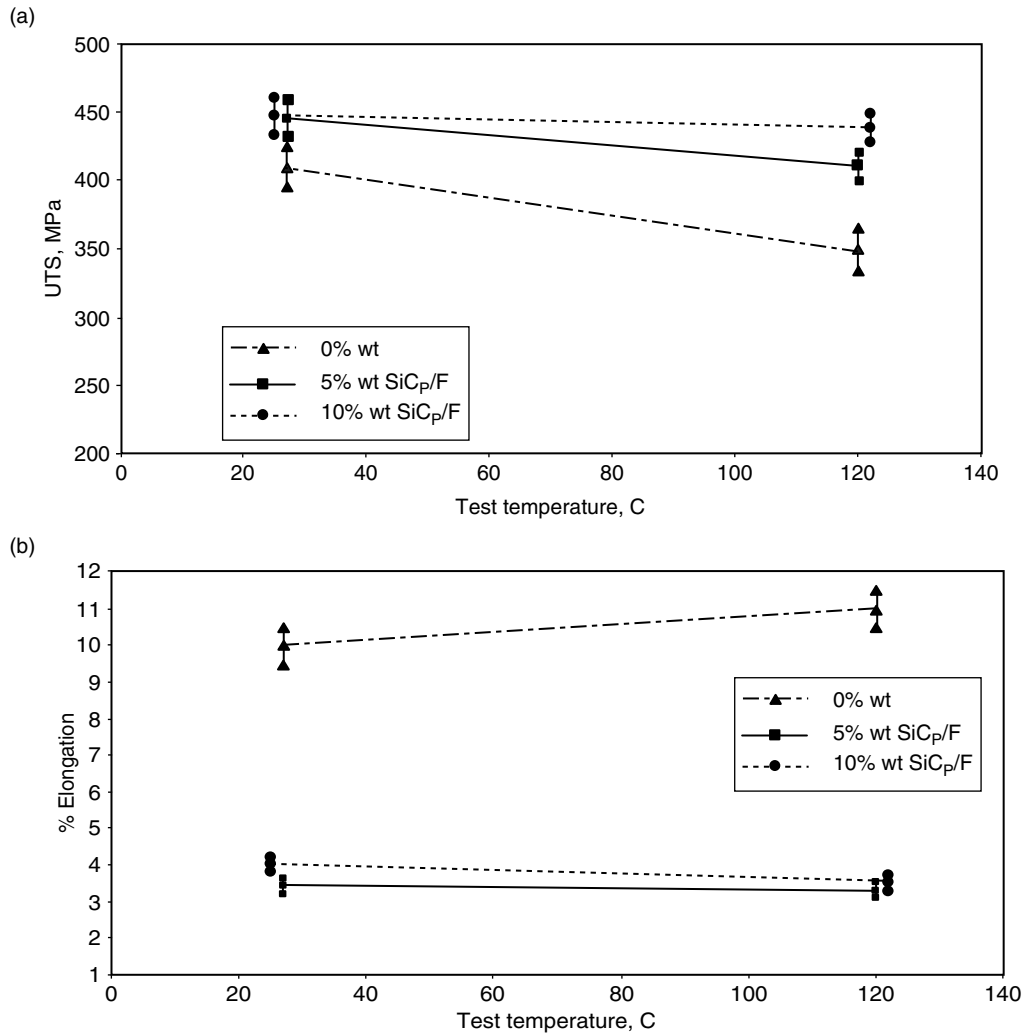


Figure 3(a). Variation of UTS with the temperature and % weight of particles. (b) Variation of % elongation with the temperature and % weight of particles.

0.2% proof strength increases with increase in weight percentages of particles. Fig. 3(a) indicates the variation of UTS with the temperature for two weight percentages of particles. From the figure, UTS of the MMC increases (5–12%) with respect to the unreinforced alloys for both weight percentages of particles at room temperature. But, the increase in UTS is significant (14–28%) at 120°C condition. At the same time, UTS increases with increase in weight percentages of particles. Fig. 3(b) presents the variation of elongation with the temperature for two weight percentages of particles. From the figure, percentage elongation of the MMC decreases (60–68%) compared to the unreinforced alloys for both (5P, 10P) weight percentages of the particles at room temperature. But the decrease in % elongation is predominant (66–72%) at 120°C condition. At the same time, % elongation shows very little reduction or almost nearly constant at room temperature and 120°C condition. The % elongation decreases with the increase in weight percentage of the particles.

The results of the tensile tests at room temperature and hot tensile test at 120°C and 200°C for particle sizes 'F' and 'C' and the unreinforced alloy are shown in Figs. 4 and 5. Fig. 4(a) shows the variation of Young's modulus with the temperature for two particle sizes. From the figure 4(a), the Young's modulus of the MMC with particle sizes 'F' is more than the MMC with particle size 'C'. Fig. 4(b) shows the variation of 0.2% proof strength with the temperature for two particle sizes. It is observed from the figure 4(b) that the 0.2% proof strength of MMC with particle size 'F' is more than the MMC with particle size 'C'. The 0.2% proof strength decreases with increase in temperature. The rate of decrease of 0.2% proof strength with respect to temperature is shallow for particle size 'C' than

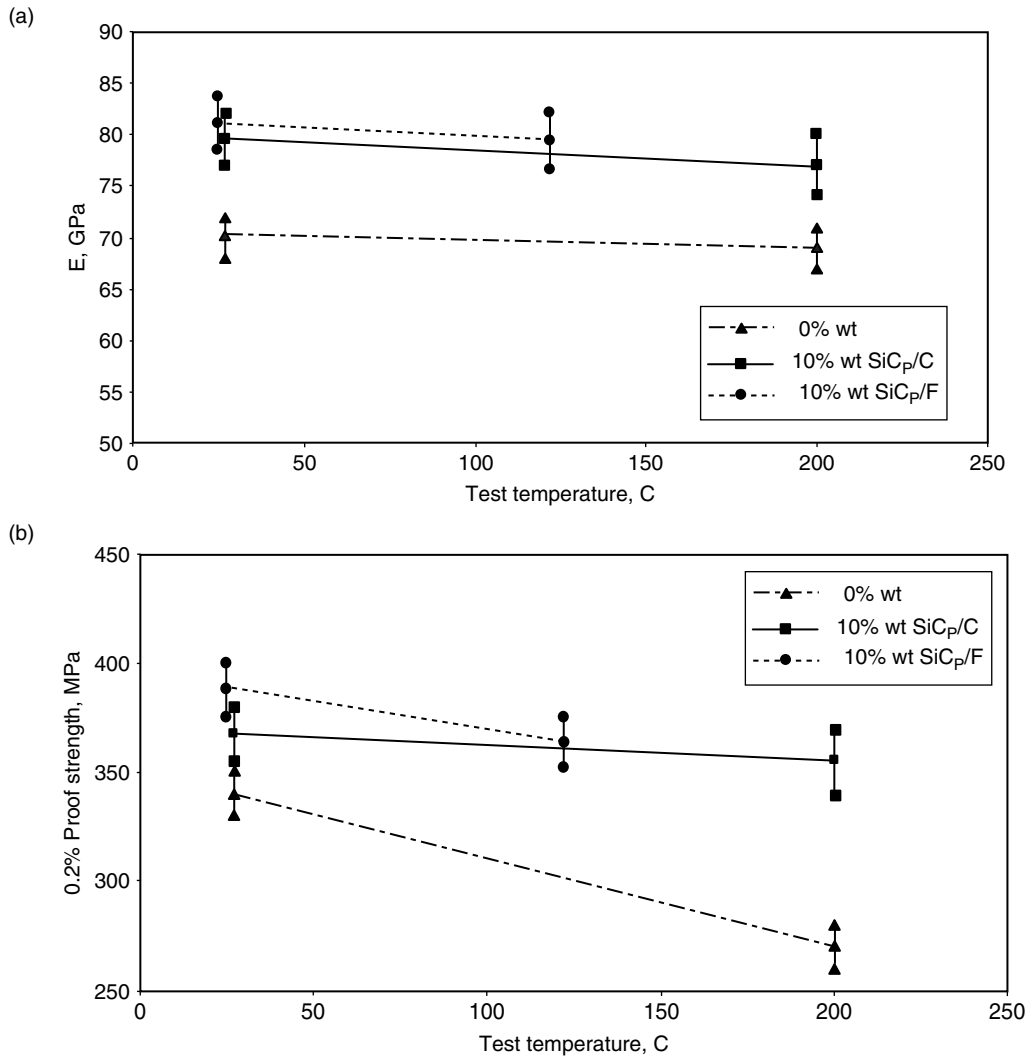


Figure 4(a). Variation of Young's modulus with the temperature and particle sizes. (b) Variation of 0.2% PS with the temperature and particle sizes.

particle size 'F'. Fig. 5(a) indicates the variation of UTS with the temperature for two particle sizes. From the figure, the UTS of MMC with particle size 'F' is more than the MMC with particle size 'C'. Fig. 5(b) indicates the variation of % elongation with the temperature for two particle sizes. From the figure, the % elongation of MMC with particle sizes 'F' is more than the MMC with particle size 'C', but the variation is insignificant.

### 3.2.1. Tensile study at room temperature

Tensile fracture of AA 2618/SiC<sub>p</sub>/F composites at room temperature was observed with dispersed SiC particles (Fig. 6a). Microscopic observations revealed the macro cracks along the transverse direction and macro voids (Fig. 6b).

Tensile fracture of AA 2618/SiC<sub>p</sub>/C composite at room temperature shows cracks and cavities on a plane normal to the far field stress axis when viewed on a macroscopic scale (Fig. 7a). SEM fracture surface (Fig. 7b) reveals a dimple structure and micro voids. The fracture mechanism is typical ductile failure.

### 3.2.2. Tensile study at 120°C

On a macroscopic scale, the tensile fracture surface of the AA 2618 / SiC<sub>p</sub>/F composites deformed at the test temperature (120°C) was flat and rough and similar to the ambient condition (Fig. 8a). Fracture surface (Fig. 8b) shows the micro voids with dimple structure. The SiC particles are uniformly distributed.

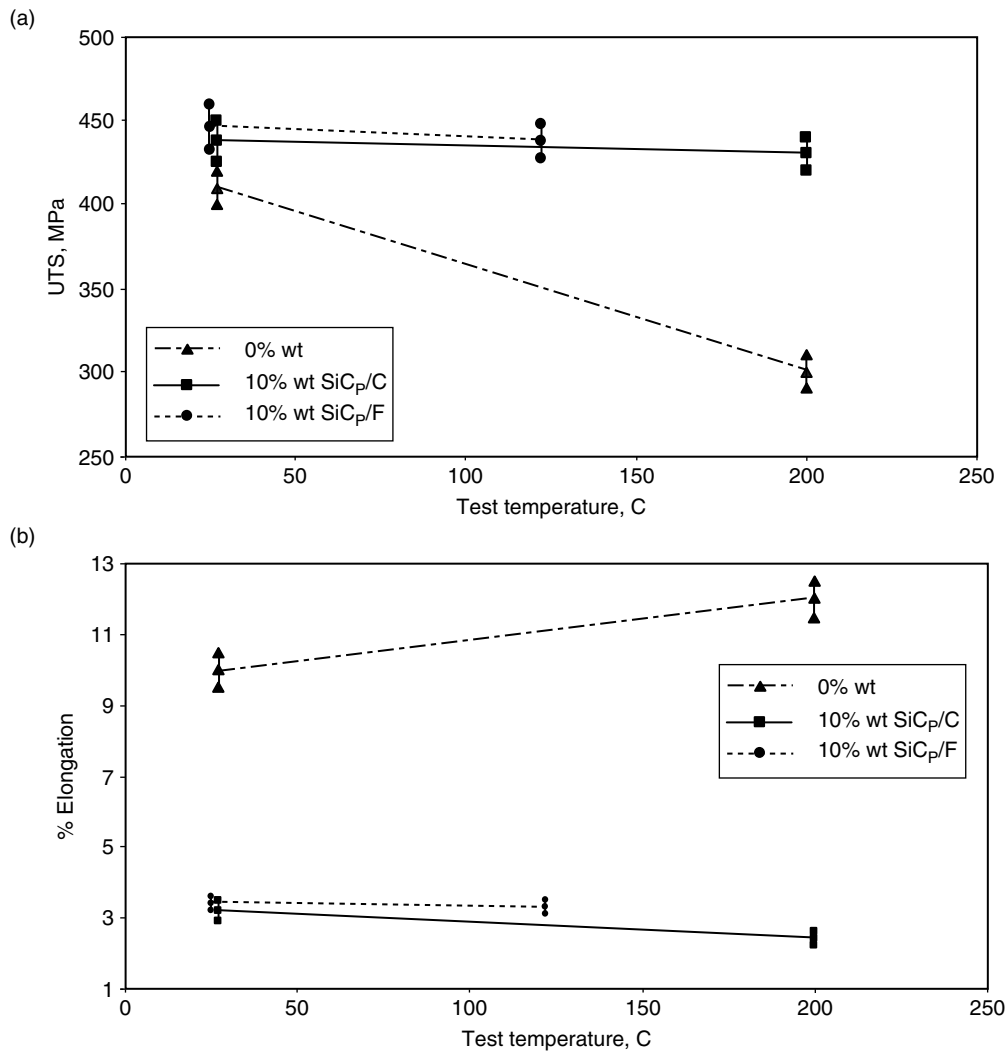


Figure 5(a). Variation of UTS with the temperature and particle sizes. (b) Variation of % elongation with the temperature and particle sizes.

### 3.2.3. Tensile study at 200°C

Tensile fracture surface of the AA 2618/SiC<sub>p</sub>/C composites at elevated temperature (200°C) was relatively rough with cracked surfaces when viewed on a low magnification (Fig. 9a). Facets and voids were noticed in the fracture surfaces, which revealed that the failure nature is micro void coalescence (Fig. 9b). High magnification observation revealed the presence of micro void coalescence with micro cracks (Fig. 9c). Fracture surface revealed the presence of micro voids throughout the surface. At higher magnification it is revealed that the fracture has micro void coalescence with dimple structure. Hence, material has ductile failure. SEM fractograph indicate the presence of agglomerated SiC particles with crack (Fig. 9d). The particles are decohered from the matrix (Fig. 9d) with ductile fracture surface. The matrix of the composites was covered with a population of microscopic voids of a wide range of sizes.

### 3.2.4. Mechanism governing tensile deformation and fracture

The constraints in mechanical deformation imposed by the hard, brittle and elastically deforming SiC<sub>p</sub> in a ductile aluminium alloy metal matrix coupled with the concurrent development of a triaxial stress state in the matrix of the AA 2618/SiC<sub>p</sub> composite is strongly limiting the flow stress of the composite microstructure and constraints in microscopic void nucleation and growth. As a direct consequence of the deformation constraints induced by the SiC<sub>p</sub> particles, a higher applied stress is required to initiate plastic deformation in the microstructure of the metal-based composites.

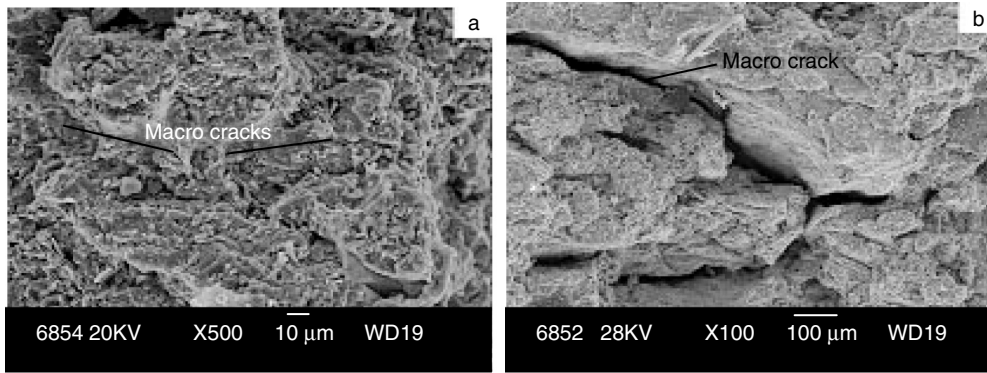


Figure 6. Scanning electron micrographs of tensile fracture surface of AA 2618/SiC<sub>p</sub>/F composites at room temperature (27°C).

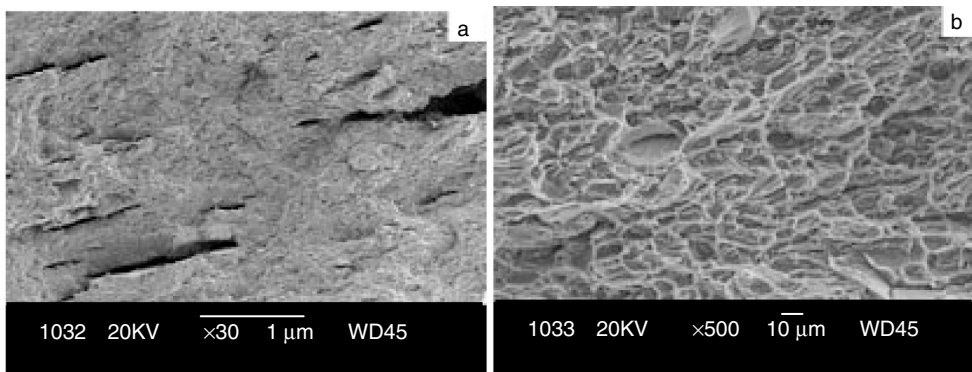


Figure 7. Scanning electron micrographs of tensile fracture surface of AA 2618/SiC<sub>p</sub>/C at room temperature (27°C).

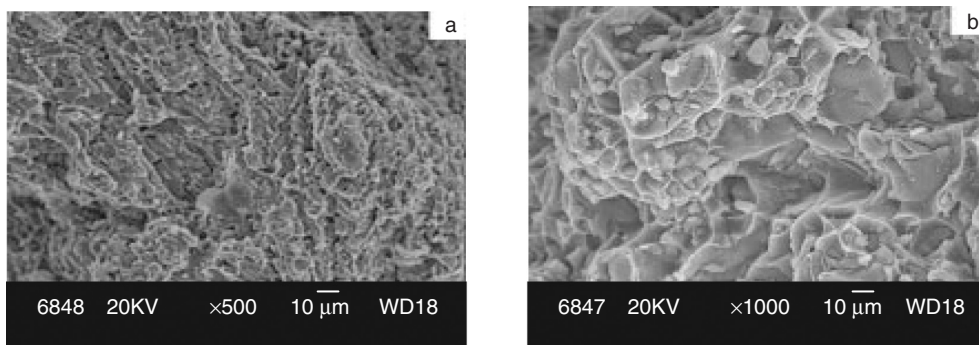


Figure 8. Scanning electron micrographs of tensile fracture surface of AA 2618/SiC<sub>p</sub>/F composites at room temperature (120°C).

Failure of the SiC particles either by cracking or decohesion at their interfaces with the Aluminium alloy metal matrix is due to the following reasons a) local plastic constraints b) particle size and c) the degree of plastic agglomeration. The local plastic constraints are particularly important for the larger size SiC particles and particle cluster during composite fracture (Fig. 9d) [22]. Examination of the tensile fracture surface revealed the damage associated with fracture localized at the discontinuous SiC particles with little evidence of void formation away from the fractured SiC particles. Fracture of the hard, brittle

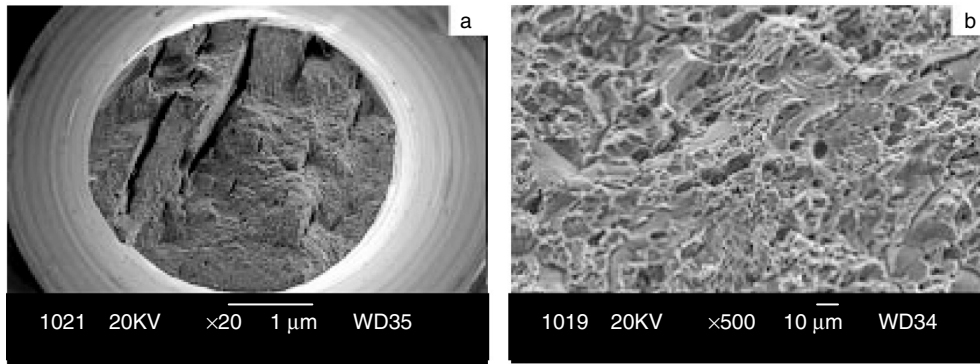


Figure 9. Scanning electron micrographs of tensile fracture surface of AA 2618/SiC<sub>p</sub>/C composites at 200°C showing a) overall morphology b) quasi-cleavage c) particle cracking and d) de-cohesion and agglomeration.

and elastically deforming SiC<sub>p</sub> was found to be greater in the regions of particle clustering. This is attributed to the a) enhanced local stresses from restriction of plastic deformation b) an intrinsic brittleness of SiC<sub>p</sub>.

The damage of the composite microstructure during uniaxial loading arising from the synergistic influences of particle cracking and decohesion at the particulate interfaces results in a detrimental influence on tensile ductility. Under the influence of an applied tensile load, micro voids are nucleated at the regions of localized strain discontinuity region such as SiC<sub>p</sub> and grain boundaries. With an increase in strain, the micro voids will grow, coalesce and finally forms a continuous fracture surface, which is a typical type of ductile failure. Formation of dimple structure with micro void coalescence is the dominant fracture mode in SiC<sub>p</sub> reinforced AA 2618.

### 3.3. High cycle fatigue

Examination was carried out on the fracture surfaces of the cyclically deformed fatigue specimens in a Scanning Electron Microscope. Fig. 10 (a) shows the shallow dimple structure of the high cycle fatigue tested specimens at 200 MPa (Cyclic load) of AA 2618/SiC<sub>p</sub>/F MMC. It shows the randomly distributed micro cracks in the region of early crack growth. High magnification fracture surface revealed the features of local brittle failure. It also reveals fine micro voids of varying size and shapes. Shallow dimple features of reminiscent of locally ductile and brittle failures are observed (Fig. 10b). The fracture surface revealed the region of stable crack growth with an array of fine microscopic cracks. The SEM fractograph (Fig. 10c) of AA 2618/SiC<sub>p</sub>/F composites cyclically deformed at the stress of 200 MPa with the resultant enhanced fatigue life ( $N_f = 2,10,000$  cycles) revealed fine striations in the region of stable crack growth with micro cracks.

#### 3.3.1. Mechanism governing cyclic deformation and fracture

For the AA 2618 metal matrix reinforced with hard, brittle and elastically deforming SiC<sub>p</sub>, the events involving the nucleation of cracks at the particulates and / or particulate cracking [13, 14, 22] tend to dominate cyclic ductility. This is because the subsequent stages of void growth and coalescence are rapid due to occurrence of both microscopic crack initiation and void initiations. An essential requirement for void nucleation is the development of a critical stress across the reinforcing SiC<sub>p</sub> and the particulate-matrix interface. The voids once nucleated tend to progressively grow with repeated cyclic straining and eventually link or coalesce culminating in fracture. The growth of macroscopic and microscopic voids is a process of cavity enlargement, which is enhanced by localized plastic deformation. Under the influence of a far field applied cyclic stress, the microscopic voids appeared to have undergone limited growth and coalescence, confirming the contribution from constraint SiC<sub>p</sub> induced triaxiality during cyclic deformation of the AA 2618/SiC<sub>p</sub> composite. The limited growth of the microscopic voids during far field cyclic loading clearly suggests that the cyclic deformation properties of 2618 aluminium alloy be altered by the presence of SiC<sub>p</sub> reinforcement.

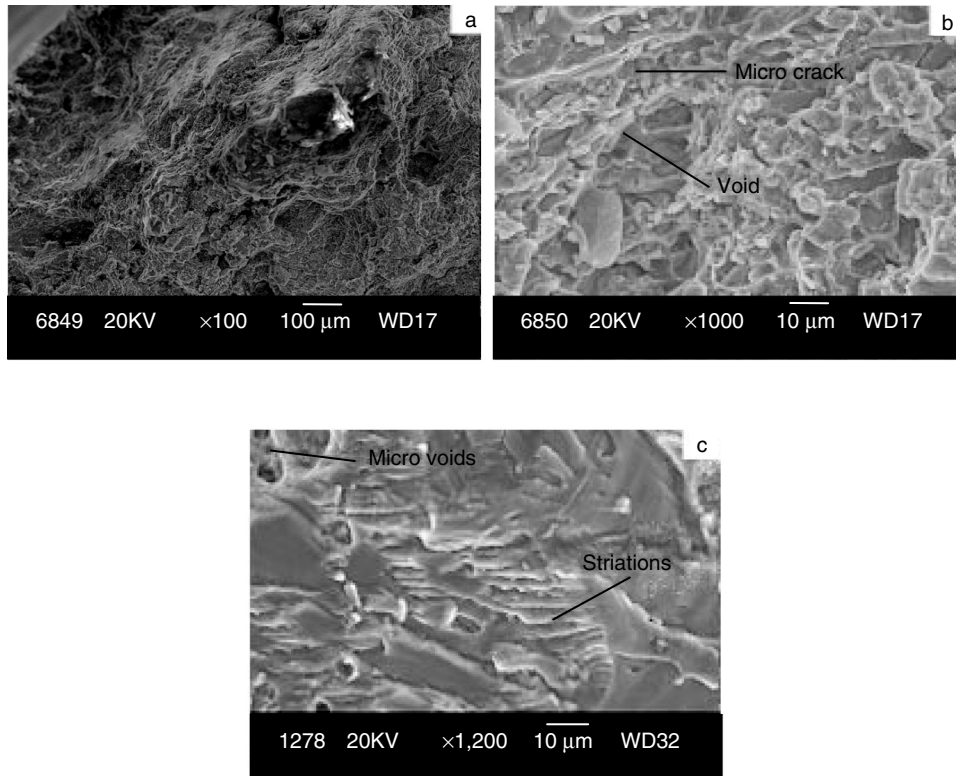


Figure 10. Scanning electron micrographs showing HCF fracture surface features of the AA 2618/ SiC<sub>p</sub>/F composite deformed at cyclic stress amplitude of 200 MPa,  $N_f = 210000$  cycles showing a) overall morphology b) microvoids, shallow dimple structure c) fine striations in the region of stable crack growth.

### 3.4. Impact behaviour of AA 2618 / SiC<sub>p</sub> composite

Izod-impact tests are carried out on all V-notched impact specimens of AA 2618/SiC<sub>p</sub> MMCs and unreinforced Al alloys. The impact strength of the Al alloy and MMCs were 5.5 to 6.5 Nm and 4 to 5.5 Nm respectively. The results showed that the impact behaviour of AA 2618/SiC<sub>p</sub> composites was significantly reduced by the presence of SiC particles. The lower impact strength of AA 2618/SiC<sub>p</sub> MMCs is attributed to the presence of brittle SiC particulate which may act as stress concentration areas. This argument is in agreement with the literature [15, 20 and 21]. Furthermore, the heterogeneous dispersion of SiC particles in the matrix resulted in the formation of clusters, which also decreased the matrix reinforcement bonding and reduced the impact strength of composites. The clustered particles were easily separated under the impact loading. This argument is supported by SEM examinations of fractured surfaces of MMC (Fig. 11a). The fracture surface shows the microvoids and voids with different shapes and sizes. Brittle and ductile features are noticed at few locations. The void nucleation around the particles (Fig. 11b) is related to interfacial debonding and the failure phenomenon indicates weak particle-matrix interface probably caused during the manufacturing process [20]. SEM fractograph (Fig. 11c) shows the cleavage ridges with particle separation from the matrix and microvoids. The fracture surface shows the cleavage planes with ridges and also cracked particles (Fig. 11c). The cracks noticed in the matrix are due to the intercrystalline failure of brittle nature. The cracks noticed in the fracture surface are intragranular in nature (Fig. 11d). These failure mechanisms have a significant effect on decreasing the impact strength of composites.

Fig. 12 shows the SEM fractograph of impact-tested specimens of AA 2618/SiC<sub>p</sub>/C composites. Fig. 12(a) shows the overall morphology of the impact specimens with rough surface and array of flow pattern in the same direction. Fig. 12(b) indicates the fracture surface with the combination of cleavage planes and dimple structure. It also contains microvoids and microcracks. Fig. 12(c) indicates the cracked fracture surfaces with particles. The particle separation/decohesion from the matrix alloy is also observed.

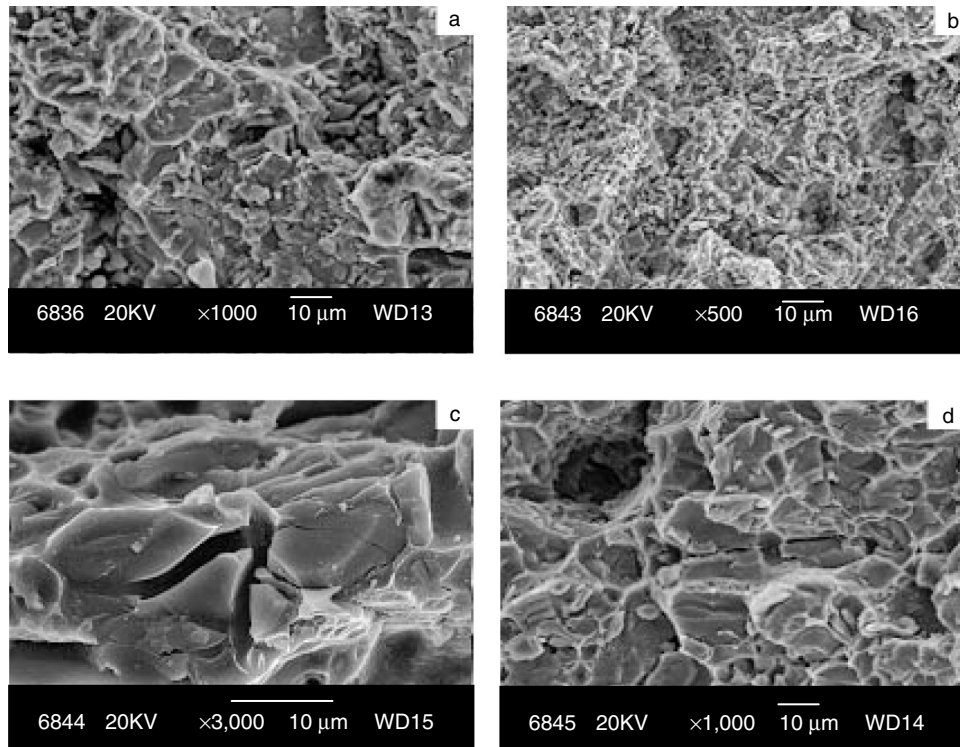


Figure 11. Scanning electron micrographs showing the impact fracture surface features of the AA 2618/SiC<sub>p</sub>/F composite showing a) clusters of particles b) void nucleation and interfacial de-bonding c) particle cracking d) inter-crystalline failure.

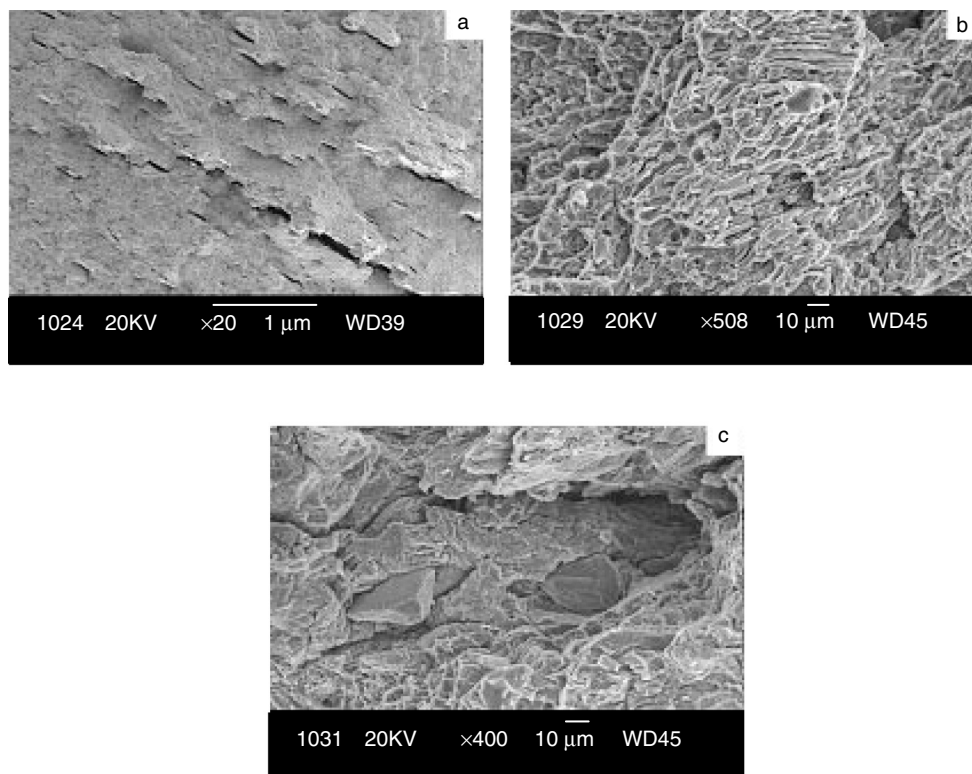


Figure 12. Scanning electron micrographs showing impact fracture surface features of the AA 2618/SiC<sub>p</sub>/C composite a) overall morphology b) cleavage plane and dimple structure c) macro cracks and de-cohesion of particles.

## 204 The Effect of Silicon Carbide Particulates on Tensile, Fatigue, Impact and Final Fracture Behaviour of 2618 Aluminium Alloy Matrix Composites

It has been observed that both clusters of particles and weak particle-matrix bonding have caused preferential directions for crack growth mechanism. This failure mechanism can be explained that the regions of clustering/agglomeration and decohesion of interface, the short inter-particle distance facilitates linkage between neighboring voids and microscopic cracks are as a direct result of decreased propagation distances between cracked SiC particles.

### 4. CONCLUSIONS

From the study of the tensile deformation, fatigue, impact resistance and final fracture behaviour of AA 2618/SiC<sub>p</sub> metal matrix composites, the following conclusions can be made:

1. The initial microstructure of the AA 2618/SiC<sub>p</sub> composites revealed a uniform distribution of SiC particles in the forging direction and good wettability is achieved in two-step mixing of stir casting method.
2. The tensile tests showed an increase in the elastic modulus and tensile strength and a decrease in the elongation to failure in the MMCs compared to the unreinforced alloys. The tensile ductility was strongly affected by the material inhomogeneity.
3. The modulus and tensile strength of the composites decreased with increasing temperature. The ductility as characterized by the elongation to failure, decreased with increasing temperature.
4. The tensile strength increased with decreasing particle size but the elongation to failure decreased with increasing particle size.
5. Extensive fractography of the failed samples revealed ductile failure with micro-void coalescence. Micro-voids are likely to be initiated at the SiC<sub>p</sub> region and grown with increase in strain on the material. However, the ductility achieved is not significant with temperature.
6. Stress amplitude fatigue life response revealed marginal enhanced fatigue life, with respect to the unreinforced alloy. Microscopic features highlighted the ductile failure by the formation of micro-voids adjacent to the SiC<sub>p</sub>. The constraint in deformation induced in the metal matrix by the SiC<sub>p</sub> particles coupled with local stress concentration effects at the matrix- particles interfaces promote failure.
7. The presence of hard, brittle SiC<sub>p</sub> particles in a ductile matrix of AA 2618 decreased the impact strength. Defects in the composite microstructure such as clustering or agglomeration of particles played a significant role in reducing the impact strength. These defects have constituted preferential sites for crack nucleation and propagation. This nucleation coupled with particle failure by cracking and debonding at the particle interfaces allowed the microscopic cracks to grow rapidly and reduces the impact strength of the composites.

### ACKNOWLEDGEMENTS

The authors wish to provide gratitude to M/s HAL (Hindustan Aeronautics Limited), Bangalore, India, for carrying out the tests pertaining to this work.

### REFERENCES

- [1] P. Cavaliere, Isothermal forging of AA 2618 reinforced with 20% of alumina particles, Composites: Part A 35(2004) 619–629.
- [2] I.N.A, Oguocha, S. Yanna Copoucas A Calorimetric study of  $S'$  and  $\theta'$  precipitation in Al<sub>2</sub>O<sub>3</sub> particle-reinforced AA 2618, Journal of Materials Science 34 (1999) 3335–3340.
- [3] Simon P. Ringer, Kazuhiro Hono, Toshio Saksai and Ian J. Polmear, Cluster hardening in an aged Al-Cu-Mg alloy, Scripta Matr. Vol. 36, (1997) 517.
- [4] S.P. Ringer, T. Sakurap and I. J. Polmear, Origins of hardening in aged Al-Cu-Mg-(Ag) alloys, ACTA Matr. Vol. 45, (1997), 3731.
- [5] R.N. Wilson and P.G. Partridge, The nucleation and growth of S precipitates in an Al-2.5%, Cu-1.2% and Mg alloy, ACTA Matr. Vol. 13, (1965), 1321.
- [6] M.K Surappa, R.K Rohatgi, Preparation and properties of cast aluminium ceramic particle composites, Journal of Materials Science 16(1981) 983–993.

- [7] G.S Hanumantha, G.A Iran, Particle incorporation by melt stirring for the production of metal matrix composites, *Journal of Materials Science* 28(1993) 2459–2465.
- [8] P. Sahin, S. Murphy, The effect of fibre orientation of the dry sliding wear of borosic reinforced 2014 aluminium alloy, *Journal of Materials Science*, 34(1996) 5399–5407.
- [9] W. Zhou, Z.M. Xu, Studies of SiC reinforced metal matrix composites, *Journal of Materials Processing Technology* 63(1997) 358–363.
- [10] L. Ceschini, G. Minak, A. Morri, Tensile and fatigue properties of AA 6061/20 Vol %  $Al_2O_3$  and AA 7005/10 Vol %  $Al_2O_{3p}$  composites, *Composites Science and Technology* 66 (2006) 333–342.
- [11] J. Hashim, L. Looney, M.S.J. Hashmi, Particle distribution in cast metal matrix composites–Part I, *Journal of Material Processing Technology* 123(2) (2002) 251–257.
- [12] T J A Doel, P Bowen, Tensile properties of particulate reinforced metal matrix composites, *Composites: Part A* 27A (1996) 655–65.
- [13] T.S. Srivatsan, M. Al. Hajri, The fatigue and final fracture behaviour of SiC particles reinforced 7034 aluminium matrix composites. *Composites: Part B* 33(2002) 391–404.
- [14] P.C. Lam, T.S. Srivatsan, Meslet al-Hajri and B. Hotton, Influence of particulate reinforcement on quasi-static and cyclic fracture behaviour of Aluminium alloy based composites. *Proceedings of Third Internal Conference on Advances in Composites, AD Comp-2000* (2000) 632–644.
- [15] D F Hasson, S M Hoover, C R Crowe, Effect of thermal treatment on the mechanical and toughness properties of extruded  $SiC_w$ /aluminium 6061 Metal matrix composites. *Journal of Materials Science*, 20 (1985) 4147–4154.
- [16] C M Friend, Toughness in metal matrix composites, *Materials Science and Technology* 5(1989)1–7.
- [17] V C Nardone, JR Strife, K M Prewo, Microstructurally toughened particulate reinforced aluminium matrix composites. *Metall, Trans* 22A (1991) 171–182.
- [18] H Ahlatci, E Candan, H Cimenoglu, Effect of Particle size on the mechanical properties of 60 Vol% SiCp reinforced Al Matrix Composites *Z. Metall, Trans* 93(4) (2002)330–333.
- [19] Sedat Ozden, Recep Ekici, Fehmi Nair, Investigation of impact behaviour of aluminium based SiC particle reinforced metal-matrix composites, *Composites Part A: Applied Science and Manufacturing* 38(2007) 484–494.
- [20] F. Bonollo, L Ceschini, G L Goragnani, Mechanical and impact behaviour of  $(Al_2O_3)_p$  / 2014 and  $(Al_2O_3)_p$  / 6061 Al metal matrix composites in the 25–200°C range. *Appl. Composite Materials* 4 (1997)173–85.
- [21] M.K Surappa, P Sivakumar, Fracture toughness evaluation of 2024-Al /  $Al_2O_3$  particulate composites by instrumented impact, *Composite Science and Technology* 46(1993) 287–92.
- [22] T.S. Srivatsan, Meslet Al Hajri, P.C. Lam, The quasi static, cyclic fatigue and final fracture behaviour of a Mg alloy metal matrix composites. *Composites- Part B*: 36(2006) 209–212.

